

Supplementary materials for

**Eco-friendly processes for the synthesis of calcium carbonate nanoparticles in ethanol and their stabilisation in aqueous media**

Lauriane Chuzeville,<sup>a,b</sup> Frank Boury,<sup>c</sup> David Duday,<sup>a</sup> Resmi Anand,<sup>a</sup> Enzo Moretto,<sup>a,b</sup> and Jean-Sébastien Thomann <sup>\*a</sup>

*<sup>a</sup>. Materials Research and Technology, Luxembourg Institute of Science and Technology, 5 Avenue des Hauts Fourneaux, Esch/Alzette L-4362, Luxembourg.*

*<sup>b</sup>. University of Luxembourg, Department of Physics & Materials Science, 162a Avenue de la faïencerie, 1511 Luxembourg city, Luxembourg.*

*<sup>c</sup>. CRCINA-GLIAD Team 17, INSERM, UMRS 1232, Université de Nantes, Université d'Angers, 49933 Angers, France.*

\*Correspondence: Tel: (+352) 27 58 88 587; Email: jean-sebastien.thomann@list.lu

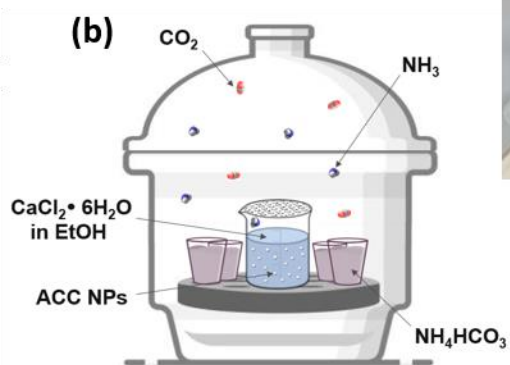
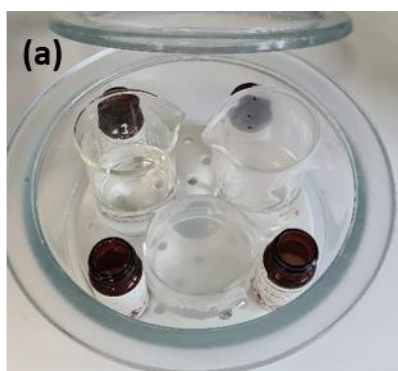


**Fig. S1 Set-up for the synthesis of ACC NPs by vacuum-assisted ADM in absolute ethanol.**

(a) Picture of the set-up inside the reaction chamber, used for the growth curves. One container diameter 4.5 cm without DB, 1 container 4.5 cm diameter with a parafilm DB punctured with 12 holes, 1 container 5.5 cm diameter with a parafilm DB punctured with 12 holes. The containers are filled with 50mL of  $\text{CaCl}_2 \cdot 6\text{H}_2\text{O}$  ethanol solution. They are surrounded by four vials containing solid ammonium bicarbonate.

(b) Schematic representation of the reaction for the synthesis of ACC NPs.

(c) Set up of the vacuum manifold (Schlenkline) used for the monitoring of the ACC NPs growth over time. Each desiccator is prepared as in (a). At  $t=0$ , the vacuum is set in the Schlenkline and in the desiccators by a vacuum pump. Once the desired value is reached, the desiccators are isolated from the Schlenkline by a valve and remain under vacuum. The pumping system stops once the desiccators are isolated. At certain time intervals, one desiccator is connected to the Schlenkline by opening the valve. The Schlenkline is connected to the ambient atmosphere, breaking the vacuum in the desiccator, and stopping the reaction. The desiccator is opened, and the solutions characterised.



**Fig. S2 Conductivity and pH follow-up set-up.**

The probes are inserted into the reaction chamber and the sealing is restored with resin or silicon. A 250 mL beaker is filled with 200 mL  $\text{CaCl}_2 \cdot 6\text{H}_2\text{O}$  ethanol solution and surrounded by 4 vials of ammonium bicarbonate. No DB is placed on the 250 mL beaker. The pH and conductivity are monitored automatically inside the solution, at different time intervals (automatic recording). When the memory is full, the recording is interrupted by disconnecting the probes from the devices. This does not alter the on-going reaction. The data are transferred to the computer. The devices are then connected back to their probes.

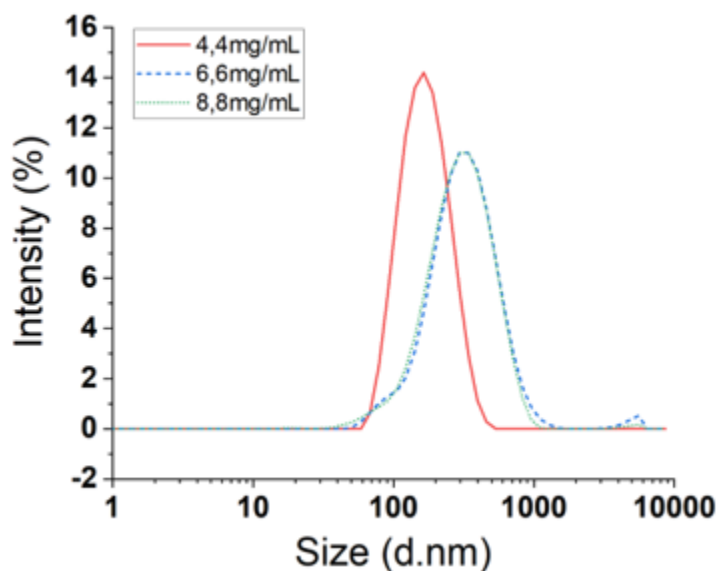


**Fig. S3 Influence of the initial concentration of  $\text{CaCl}_2 \cdot 6\text{H}_2\text{O}$ .**

The initial concentration of  $\text{CaCl}_2 \cdot 6\text{H}_2\text{O}$  is known to influence the formation of ACC NPs in aqueous ADM. Several initial concentrations of calcium chloride have been tested in pure ethanol ADM. The results evidence ACC NPs with a narrower size distribution and a smaller mean diameter for an initial concentration of  $4.4 \text{ mg} \cdot \text{mL}^{-1}$  compared to other concentrations. The difference is significant, showing a shift to higher sizes with the formation of aggregates, visible on the micrometre range of the size distribution.

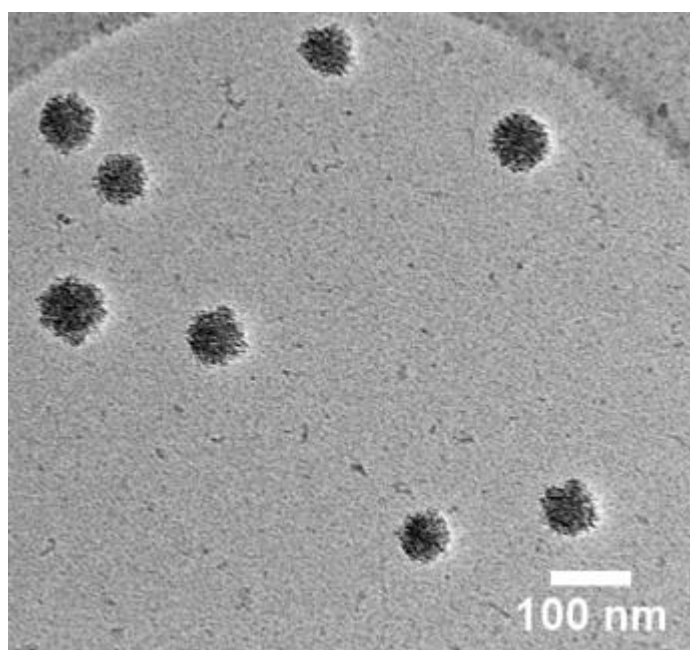


**Fig. S4 CryoTEM characterisation of ACC NPs in ethanol.**

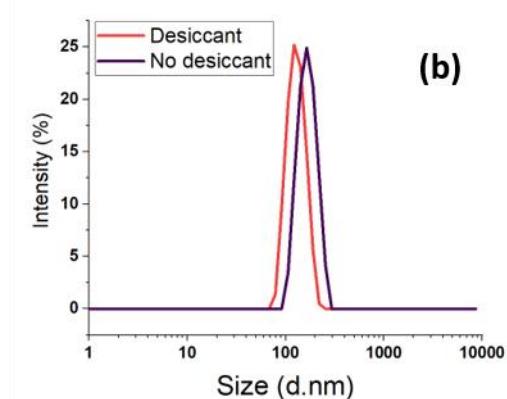


**Fig. S5 Influence of the presence of desiccant in the chamber on samples synthesised with a DB on the  $\text{CaCl}_2 \cdot 6\text{H}_2\text{O}$  solution container.**

Initial  $\text{CaCl}_2 \cdot 6\text{H}_2\text{O}$  concentration:  $4.4 \text{ mg} \cdot \text{mL}^{-1}$ , initial volume 50mL. The diffusion barriers were punctured with the same number of holes. (a) ACC NPs final solution synthesised with desiccant (right) and without desiccant (left). (b) DLS size distribution characterisation of the ACC NPs solution synthesised with and without desiccant in the chamber. The size dispersion is not significantly impacted (PDI similar, with and without desiccant 0.019 and 0.012, respectively). The nanoparticles synthesised without desiccant are larger, at 162 nm, than those with desiccant (126 nm). The final mass concentration is greatly affected (mass concentration with desiccant:  $0.2 \text{ mg} \cdot \text{mL}^{-1}$ , and without desiccant:  $0.1 \text{ mg} \cdot \text{mL}^{-1}$ ). The solution turbidity is significantly higher without desiccant.

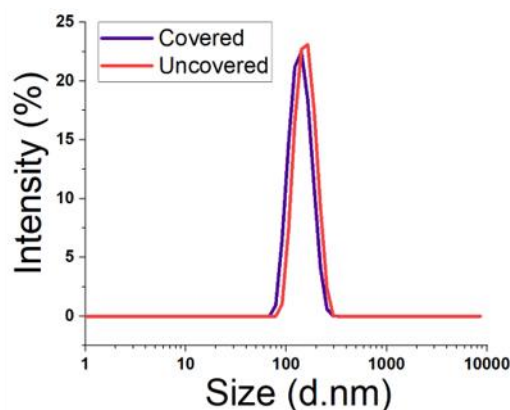
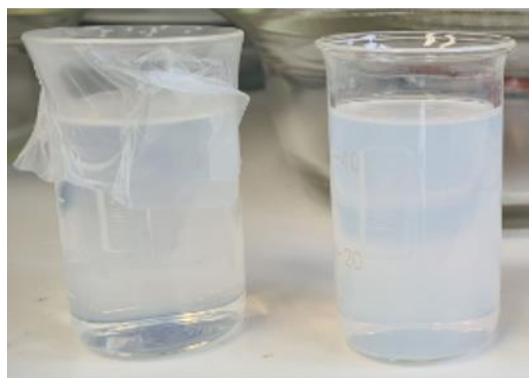


**Fig. S6 Influence of the presence of a DB on the synthesis of ACC NPs.**

Initial  $\text{CaCl}_2 \cdot 6\text{H}_2\text{O}$  concentration:  $4.4 \text{ mg} \cdot \text{mL}^{-1}$ , initial volume 50mL. (a) ACC NPs final solution synthesised with a DB (left) and without a DB (right). (b) DLS size characterisation of the ACC NPs solutions synthesised with a DB and without. No significant size or size dispersion variation is observed. The final mass concentration is however impacted (mass concentration with a DB:  $0.5 \text{ mg} \cdot \text{mL}^{-1}$ , and without a DB:  $1.2 \text{ mg} \cdot \text{mL}^{-1}$ ). The solution turbidity is also higher without a DB.

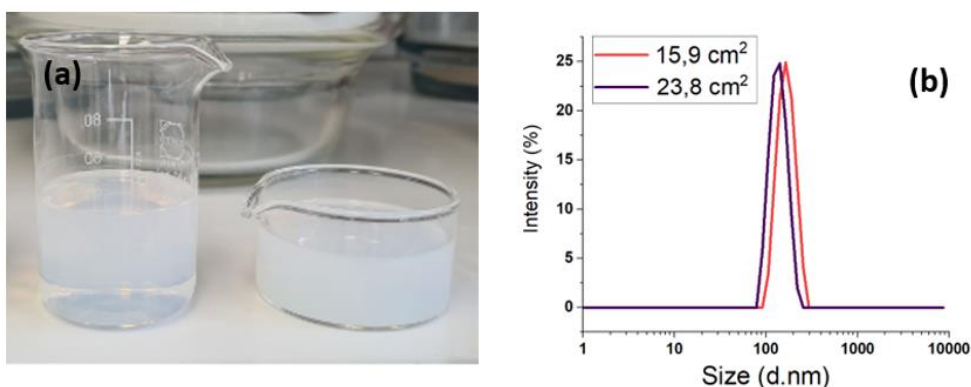


**Fig. S7 Influence of the size variation of the diffusion area between the vacuum chamber atmosphere and the  $\text{CaCl}_2 \cdot 6\text{H}_2\text{O}$  solution.**

Initial  $\text{CaCl}_2 \cdot 6\text{H}_2\text{O}$  concentration:  $4.4 \text{ mg} \cdot \text{mL}^{-1}$ , initial volume 50mL. The diffusion barriers were punctured with the same number of holes. The diffusion area is linked to the diameter of the  $\text{CaCl}_2 \cdot 6\text{H}_2\text{O}$  solution container. Containers of 4.5 cm and 5.5 cm diameter were used, representing diffusion areas of  $15.9 \text{ cm}^2$  and  $23.8 \text{ cm}^2$  respectively.

(a) ACC NPs final solution synthesised with diffusion area of  $15.9 \text{ cm}^2$  (left) and  $23.8 \text{ cm}^2$  (right).

(b) DLS size characterisation of the ACC NPs solutions synthesised with diffusion area of  $15.9 \text{ cm}^2$  and  $23.8 \text{ cm}^2$ . No significant size or size dispersion variation is observed. A size increase of 5 nm is noticed with the increase of the diffusion area. The solution turbidity is similar for both samples. The final mass concentration is significantly lower for the samples synthesised with a larger diffusion area (mass concentration for a diffusion area of  $15.9 \text{ cm}^2$ :  $1.1 \text{ mg} \cdot \text{mL}^{-1}$ , mass concentration for a diffusion area of  $23.8 \text{ cm}^2$ :  $2.1 \text{ mg} \cdot \text{mL}^{-1}$ ).

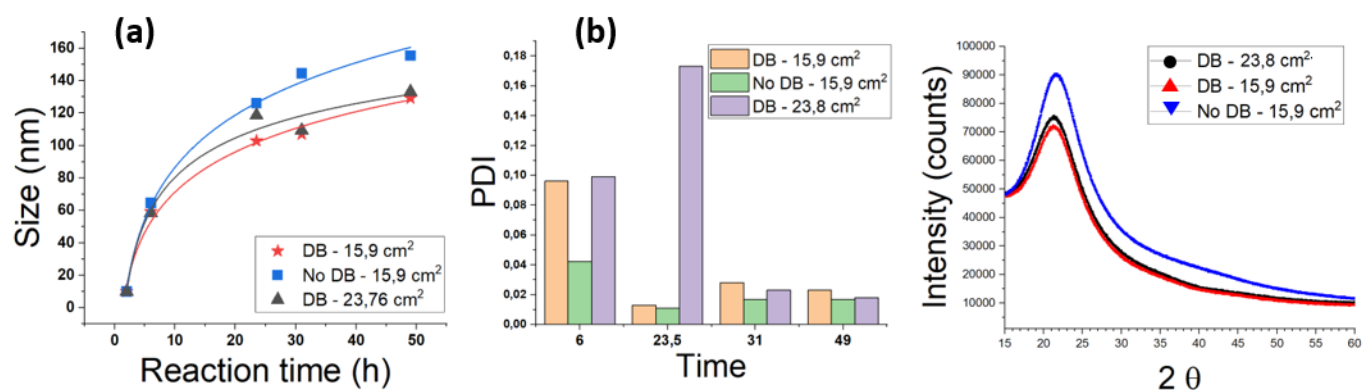


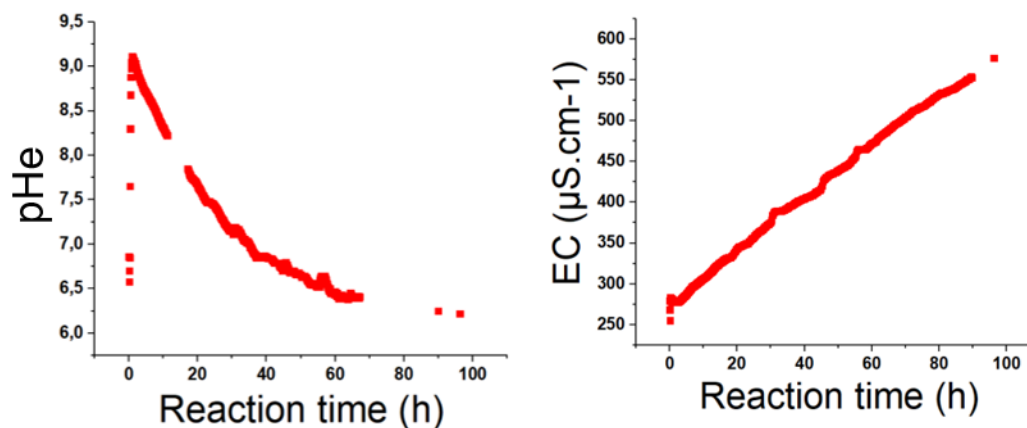
**Fig. S8 ACC NPs growth depending on the reaction time – Second Experiment to confirm the trends.**

For each sample, initial  $\text{Cl}_2 \cdot 6\text{H}_2\text{O}$  concentration:  $4.4 \text{ mg} \cdot \text{mL}^{-1}$ , initial volume: 50mL.

(a) ACC NPs growth curves showing the average size increase with time. *Black*: container providing an ethanol/gas interface of  $15.9 \text{ cm}^2$ , covered with parafilm punctured with small holes. *Blue*: container providing an ethanol/gas interface of  $23.8 \text{ cm}^2$ , covered with parafilm punctured with small holes. *Red*: container providing an ethanol/gas interface of  $15.9 \text{ cm}^2$ , uncovered.

(b) PDI related to experiment (a), for different reaction time.

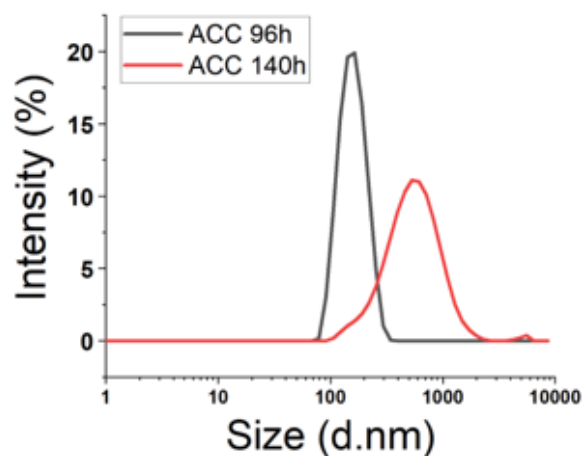
(c) XRD spectra for the different samples. *Red*: container providing an ethanol/gas interface of  $15.9 \text{ cm}^2$ , covered with parafilm punctured with small holes. *Black*: container providing an ethanol/gas interface of  $23.8 \text{ cm}^2$ , covered with parafilm punctures with small holes. *Blue*: container providing an ethanol/gas interface of  $15.9 \text{ cm}^2$ , uncovered.



**Fig. S9 pH and conductivity monitoring for the growth of ACC NPs.**

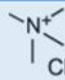
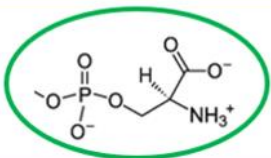
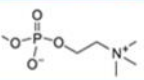
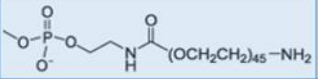
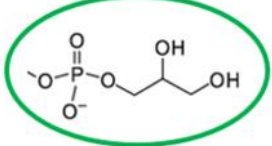
Monitoring of the pH and conductivity during the ACC NPs synthesis for 96h.

Left: pH evolution with time. Right: conductivity evolution with time.



**Fig. S10** Size dispersion characterised by DLS after 96h and 140h reaction time.

Size at 96h and 140h reaction time characterised by DLS. At 140h, polydisperse population with 2 size populations and a high polydispersity index (0.257).

Lipid	Polar head structure
18:1 TAP	
18:1 PS	
16:0 PS	
16:0 PC	
16:0 PC + DSPE-PEG (80/20 w/w)	
16:0 PG	
EPG (*C12-C24 + C12-C24 unsaturated)	

**Fig. S11** Lipid head groups

Lipids and lipid mixes used as stabilisers and their polar head structure. The green circles represent the polar head structures, which provide an effective stabilisation of ACC NPs in aqueous media with an ethanol injection method. The affinity for calcium ions and positive surface charges comes from their negative charge and OH groups. The zwitterionic and positive head groups did not provide effective stabilisation with our process.



**Fig. S12 Comparative table of the different existing processes for the stabilisation of calcium carbonate nanoparticles in water**

Parameters impacting the sustainability of the process

Article	CaCO <sub>3</sub> -phase	Mean size	Stability	Size homogeneity Standard deviation (SD) from SEM, PDI from DLS, or size values from the article text	PEGylated materials	Toxic solvents	Synthetic polymers	Bio-sourced stabiliser	Process time
Liposomes-assisted synthesis <sup>1,2</sup>	Amorphous	15-470nm	20h	27nm +/- 7nm <sup>1</sup> or 130nm +/- 50nm <sup>2</sup>	No	Yes	No	Yes	> 30 minutes
Liposome-assisted synthesis <sup>3,4</sup>	Vaterite and calcite	> 1µm	N/A	Mean 1.7µm SD > 780nm <sup>4</sup> , or mean 21.5µm SD >10µM <sup>3</sup> )	No	Yes	No	No	> 25 hours
Wang <i>et al.</i> <sup>5</sup> (ethanol injection)	Amorphous	100 nm	24h	~100nm, small PDI (from article text)	Yes	No	No	No	24 hours
Park <i>et al.</i> <sup>6</sup> (Biom mineralisation)	Vaterite-polymer hybrid	300 nm	N/A	354nm +/-59.5nm, PDI 0.24	Yes	Yes	Yes	No	48 hours for the polymer synthesis + 17h for the particles
Huang <i>et al.</i> <sup>7</sup> (Biom mineralisation)	N/A – Hybrid CaCO <sub>3</sub> -Polymer	200 nm	At least 4h	212.6nm +/- 10.1nm, PDI 0.126	No	No	Yes	No	17 hours
Vidallon <i>et al.</i> <sup>8</sup> (Polymer)	Vaterite	550 nm	N/A	575nm +/- 30.73nm	No	No	Yes	No	15 minutes, + 100min for RBC membrane coating
Tanaka <i>et al.</i> <sup>9</sup> (Polymer)	Vaterite - Hybrid CaCO <sub>3</sub> -Polymer	360 nm or more	40h with size of 600 to 800nm	360nm +/- 180nm	No	Yes	Yes	No	> 72 hours
Xu <i>et al.</i> <sup>10</sup> (Biom mineralisation)	Amorphous Hybrid CaCO <sub>3</sub> -Polymer	60 nm	1 month	62nm +/- 10nm	No	No	Yes	No	1,5-4,5 hours
<b>Our process (ethanol injection)</b>	<b>Amorphous</b>	<b>120nm</b>	<b>3 months</b>	<b>148.7nm PDI 0.022 for Egg-PG</b>	<b>No</b>	<b>No</b>	<b>No</b>	<b>Yes</b>	<b>2 minutes</b>

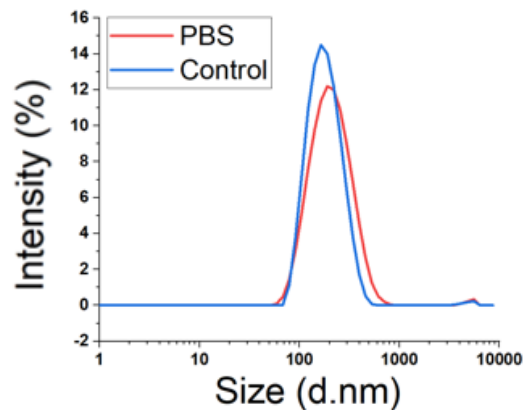


**Fig. S13 Stabilisation ACC NPs in PBS**

DOPS-LCC NPs size dispersion characterised by DLS after stabilisation in PBS (red) and in water, used as a reference (blue). A size shift is observed from 168.5nm water to 187.3nm in PBS with a PDI increase from 0.15 to 0.21.

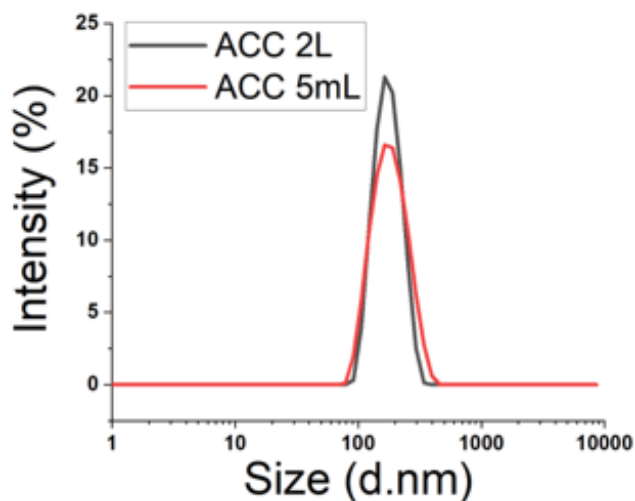


**Fig. S14 Upscaling - Size dispersion characterised by DLS for pipetting injection (5mL) and magnetic stirring protocol (2L).**

Both size dispersions are narrow and centred on similar sizes. PDI for 5mL is 0.091 and for 2L 0.042.

- 1 Tester, C. C., Wu, C.-H., Weigand, S. & Joester, D. Precipitation of ACC in liposomes—a model for biomineralization in confined volumes. *Faraday Discussions* **159**, 345-356 (2012).
- 2 Tester, C. C. *et al.* In vitro synthesis and stabilization of amorphous calcium carbonate (ACC) nanoparticles within liposomes. *CrystEngComm* **13**, 3975-3978 (2011).
- 3 Szcześ, A. Effect of the enzymatically modified supported dipalmitoylphosphatidylcholine (DPPC) bilayers on calcium carbonate formation. *Colloid and polymer science* **294**, 409-419 (2016).
- 4 Szcześ, A. Effects of DPPC/Cholesterol liposomes on the properties of freshly precipitated calcium carbonate. *Colloids and Surfaces B: Biointerfaces* **101**, 44-48 (2013).
- 5 Wang, C. *et al.* Facile preparation of phospholipid–amorphous calcium carbonate hybrid nanoparticles: toward controllable burst drug release and enhanced tumor penetration. *Chemical Communications* **54**, 13080-13083 (2018).
- 6 Park, D. J. *et al.* Photosensitizer-loaded bubble-generating mineralized nanoparticles for ultrasound imaging and photodynamic therapy. *Journal of Materials Chemistry B* **4**, 1219-1227 (2016).
- 7 Huang, H., Zhang, W., Liu, Z., Guo, H. & Zhang, P. Smart responsive-calcium carbonate nanoparticles for dual-model cancer imaging and treatment. *Ultrasonics* **108**, 106198 (2020).
- 8 Vidallon, M. L. P. *et al.* Gas-Generating, pH-Responsive Calcium Carbonate Hybrid Particles with Biomimetic Coating for Contrast-Enhanced Ultrasound Imaging. *Particle & Particle Systems Characterization* **37**, 1900471 (2020).
- 9 Tanaka, Y. & Naka, K. Synthesis of calcium carbonate particles with carboxylic-terminated hyperbranched poly (amidoamine) and their surface modification. *Polymer journal* **44**, 586-593 (2012).
- 10 Xu, C. *et al.* Biodegradable Nanoparticles of Polyacrylic Acid–Stabilized Amorphous CaCO<sub>3</sub> for Tunable pH-Responsive Drug Delivery and Enhanced Tumor Inhibition. *Advanced Functional Materials* **29**, 1808146 (2019).